Fabrication of a nanofiber membrane functionalized with molecularly imprinted polymers for humic acid removal from peat water

M.A. Zulfikar[a,*], I. Afrianingsih[a], M. Nasir[b], N. Handayani[a]

[a]*Analytical Chemistry Research Group, Institut Teknologi Bandung, Jl. Ganesha 10, Bandung 40132, Indonesia,*
Tel. +62-22-2502103; Fax: +62-22-2504154; emails: zulfikar@chem.itb.ac.id (M.A. Zulfikar), irlin89@gmail.com (I. Afrianingsih),
nurrahmi.105@gmail.com (N. Handayani)
[b]*Research Center for Chemistry, Indonesian Institute of Sciences (LIPI), Jl. Cisitu-Sangkuriang, Bandung 40135, Indonesia,*
email: mnasir71@yahoo.com

a b s t r a c t

The potential of nanofiber membrane functionalized with molecularly imprinted polymers (NFMIPs) prepared by the electrospinning technique for the humic acid (HA) removal from peat water was investigated. In this process, preparation of NFMIPs comprised of two steps. The first step was to synthesize fabrication of polyvinylidene fluoride (PVDF) nanofiber membrane as support and the second step was to synthesize imprinted polymer on the surface of PVDF nanofiber membrane. The prepared NFMIPs were characterized by Fourier transform infrared spectroscopy, scanning electron microscopy, transmission electron microscopy, Brunauer–Emmett–Teller and thermogravimetric analysis. Finally, the adsorption experiments were carried out to investigate the effect of different adsorption parameters, such as contact time, adsorbent dosage, pH and temperatures in a batch system. The NFMIPs materials were then used for HA adsorption from peat water using batch adsorption technique. Adsorption was best described by Langmuir isotherm and adsorption capacity was found to be 153.3 mg/g. From the kinetic studies, the adsorption of HA onto NFMIPs materials followed the pseudo-second-order kinetic model with a rate constant in the range of 0.032–0.104 g/mg min. The adsorption equilibrium was achieved at about 90 min. The amount adsorbed increased with increasing adsorbent dosage and the temperature, otherwise decreased with increasing peat water pH (from 2 to 10).

Keywords: Electrospinning; Humic acid; Nanofiber; Peat water

1. Introduction

Humic acid (HA) is a major component of natural organic substances and it can be identified in the peat water. HA affects water quality, such as color, taste and odor. HA not only reacts with disinfectants to produce disinfection by-products harmful to human health, but also could enhance the transport of some persistent organic pollutants such as polycyclic aromatic hydrocarbons to aquatic organisms [1]. Thus, removal of HA from surface water or wastewater is very important.

HA removal from surface water may involve several methods that have been founded by previous researcher, such as photocatalysis [2], electrocoagulation [3], biofiltration [4], coagulation–flocculation [5] and membrane technology [5,6]. However, these techniques are associated with problems such as excessive time requirements, high costs and high energy consumption [7].

Adsorption process is of high interest due to its efficiency, flexibility and simplicity of design, and ease of operation [8,9]. The adsorbent is one of the key factors during the course of adsorption in determining the effectiveness of adsorption processes; hence, it has become an important research direction to find a suitable adsorbent for the removal of HA. For HA, until now, various natural and synthetics adsorbents

* Corresponding author.

have been studied, such as activated carbon [10,11], fly ash [12], *Shorea dasyphylla* sawdust [13], eggshell [14], zeolite [15], clay mineral [16,17], chitosan and chitin [18,19], silica [20] and other adsorbents [21–23]. However, the deficiencies of the abovementioned adsorbents, such as ordinary adsorption capacities and poor regeneration abilities, confine their extensive use in the practice of water/wastewater treatment. Therefore, it is imperative to develop a new high-efficient adsorbent for removal of HA from peat water.

Certain properties such as high mechanical, thermal stability, surface area and high sorption capacity should be carefully considered for the adsorbent. The nanofiber membranes prepared by the electrospinning method have unique properties, such as high specific surface area, great porosity with fine pores as well as easy handling. Because of its unique properties, the electrospin nanofiber materials have been developed for protein/enzyme purification [24,25], removal of heavy metal ions [26–28] and dyes [29–31].

Molecular imprinting technique (MIT) was carried out based on the principle of polymerization between template molecule and functional monomer to prepare molecular imprinting polymers (MIPs) with specific binding sites which can identify template molecule, and these sites are complementary with template molecule in the shape and spatial structure [32,33]. MIT has been applied in many fields, such as environmental samples, or food and beverage samples [23,32–34]. However, most studies until now still have some defects, such as long adsorption time, low adsorption capacity, low selectivity, low response kinetics and poor site accessibility [33,35]. Surface imprinting technique has been proposed as an improved MIT to overcome some of these weaknesses [33,36]. This technique is to prepare MIPs on the surface of solid matrix for obtaining regular MIP composites with abundant binding sites and cavities on the solid surface. Therefore, in this work, we explored a modified surface imprinted technique to produce hollow polymer with larger spaces for easy accessing by removing the matrix of prepared MIPs.

This study reports the fabrication of nanofiber membrane functionalized with molecularly imprinted polymers (NFMIPs) by electrospinning process and its application as an adsorbent for the removal of HA from peat water. Besides, the study further investigated the effects of various experimental conditions, such as contact time, pH, adsorbent dosages and temperature on the HA removal process. In order to understand the characteristics of the removal process, the adsorption isotherms, kinetics and thermodynamics have also been performed.

2. Materials and methods

2.1. Materials

Polyvinylidene fluoride (PVDF) with higher molecular weight was purchased from Aldrich (St. Louis, USA) and dried at 50°C under vacuum condition for at least 24 h before use. Methyl methacrylate (MMA) as a monomer, HA as templates, ethylene glycol dimethacrylate (EGDMA) as a cross-linker, 2,2-azobisisobutyronitrile (AIBN) as an initiator, dimethylformamide (DMF) and dimethylacetamide (DMAc) as a solvent were purchased from Merck (USA). All materials

were commercial reagent grade and used as received without further purification. Deionized water was used in all experiments. Peat water sample was obtained from Panam, a subdistrict of Pekanbaru in Riau Province, Indonesia. The characteristics of peat water sample are shown in Table 1.

2.2. Synthesis of PVDF nanofiber membrane as support

First, PVDF polymer dope solutions for electrospinning were prepared by dissolving PVDF (12%) in DMAc. A desired amount of LiCl (0.004 wt%) was added into dope solutions to improve dope electrospin ability, optimize the electrospun nanofiber membranes porosity and control membrane pore sizes. The dope solutions were stirred mechanically for at least 24 h at 60°C. The homogenous dope solutions were then cooled down and degassed at room temperature for overnight before electrospinning.

Fig. 1 shows schematic diagram of an electrospinning setup. Basically, the homogenous solution of PVDF was put in a syringe (needle diameter 0.6 mm). The positive terminal of a high voltage power supply was connected to the metallic syringe tip while the negative terminal was connected to a conductive drum covered with aluminum foil as a collector of fibers. A voltage of 15 kV and a speed of 0.7 mL/min were applied across a distance of 12 cm between the tip of the sprayers and the grounded collector aluminum foil. During electrospinning process, nanofibers were produced and collected on non-woven textiles posted on the rotating collector when the applied electric field overcomes the surface

Table 1
The characteristic of peat water sample

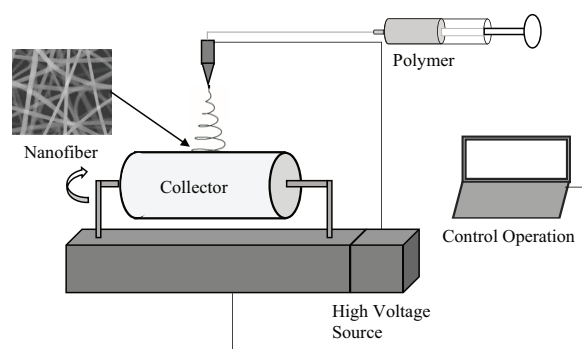| Parameters	Result
Color, Pt–Co	482
Organic compounds, mg/L KMnO$_4$	245
pH	3.95
Conductivity, μS/cm	78
Turbidity, mg/L SiO$_2$	7.2
Iron, mg/L	0.28
Manganese, mg/L	0.12
Calcium, mg/L	0.04
Magnesium, mg/L	6.2

Fig. 1. Schematic diagram of an electrospinning setup.

tension of the polymer dope solution. Solvents in the nascent nanofibers were evaporated and nanofibers started to bend concurrently. In order to eliminate the effect caused by the residual solvent in the membrane, the PVDF ENMs were subsequently placed in a fume cupboard under vacuum condition at 60°C for overnight to ensure that all solvents have been evaporated completely from the fresh membranes.

2.3. Synthesis of PVDF nanofiber membrane functionalized with MIPs

The functionalized reaction solution was prepared by blending of 5 mmol of MMA (0.500 g), 20 mmol of EGDMA (4.20 g) and 100 mg of AIBN to HA as a template. This solution was mixed with 5.116 g of nanofibers and 31 mL of preheated DMF in a 100 mL three-necked flask and continuously stirred at 60°C for 24 h. The reaction was performed under an inert atmosphere of nitrogen (99.99%). The final fibrous product was suction filtered, washed with deionized water until no sulfur ions were detected in the washing solution, and dried in a vacuum oven at 60°C. About 3 g of these fibers were subjected to leaching with 200 mL of 5 M HNO_3 for 5 h to obtain MIPs material, and then washed with methanol. After washing, the nanofibers were dried by means of vacuum, after which they were ready for use.

2.4. Material characterizations

The IR spectrum of PVDF nanofiber membrane and NFMIPs was examined by the Fourier transform infrared spectroscopic (FTIR) spectrophotometer model 8300 IR-TF (Shimadzu, Japan), equipped with both horizontal attenuated total reflectances accessories operating in the wave number range of 4,000–400 cm^{-1}. X-ray diffraction (XRD) measurements were carried out to characterize the crystalline phase of PVDF nanofiber and NFMIPs with a PANalytical X-ray diffractometer X'Pert Pro with Cu Ka radiation at 40 kV/30 mA. The diffractograms were scanned in a 2θ range of 10°–70° at a rate of 2°/min. The surface morphology of PVDF nanofiber and NFMIPs was investigated using a scanning electron microscopy (SEM; JSM-6360 LV, Japan). The surface area of the both PVDF nanofiber and NFMIPs was measured using Brunauer–Emmett–Teller (BET) analyzer (Micromeritics Gemini III 2375, USA). Pore-size distributions were calculated using the Barrett–Joyner–Halenda (BJH) model based on the nitrogen desorption isotherm by a porosimeter (Autoporel V 9500, Micromeritics Co., USA). Contact angles of the nanofiber substrates were measured based on sessile drop method, using a goniometer (Contact Angle System OCA, DataPhysics Instruments GmbH, Germany).

2.5. Adsorption studies

The removal of HA from peat water was investigated by batch method. Each samples (0.05 g) of dried PVDF nanofiber and NFMIPs were added to 50 mL peat water sample in a 100 mL Erlenmeyer flasks which were agitated at a constant speed of 100 rpm in thermostatic shaker bath (Innova 3000). The effect of contact time on the adsorption by both samples was studied for different intervals of time ranging from 5 to 120 min at room temperature. At the end

of the run, both samples were removed and solution was centrifuged at 4,000 rpm for 30 min. The HA concentration in the clear solution in mg/L was determined using ultraviolet–visible spectrophotometer model UV–Vis 1601 (Shimadzu, Japan) at the λ 400 nm [14,23]. The percentage adsorption of HA and adsorption capacity of PVDF nanofiber and NFMIPs were calculated, respectively, using the following equations:

$$\% \,\text{Adsorption} = \frac{C_i - C_e}{C_i} \times 100 \tag{1}$$

$$q_e \,(\text{mg/g}) = \frac{C_i - C_e}{m} \times V \tag{2}$$

where C_i and C_e are the initial and final concentration of HA (mg/L) in solution, respectively; V is the volume of solution (L) and m is the mass of materials (g) used.

The effect of adsorbent dosage (0.01–0.1 g) on the HA removal from peat water was investigated by contacting 50 mL of peat water at pH 4 and room temperature for 60 min. The next procedure was similar to that of the effect of agitation time. The effect of pH on HA removal was studied by contacting 50 mL of peat water at varying the pH from 2.0 to 11.0 for 60 min at room temperature. The pH of the peat water sample was adjusted using 0.1 M HCl or 0.1 M NaOH and measured by using a pH meter (Orion Aqualytic AL15). For examining the effect of temperature on HA removal, 0.05 g of the adsorbent was immersed in 50 mL of peat water at four different temperatures (25°C, 45°C, 65°C and 85°C). The next procedure was similar to that described for the effect of agitation time.

3. Results and discussion

3.1. Characterization of adsorbents

FTIR spectra were used to detect the surface functional groups of sample, as shown in Fig. 2. As shown in Fig. 2(a), three strong peaks at 1,404, 880 and 1,183 cm^{-1} were observed in PVDF nanofiber absorption band. The former two peaks were obtained from C–F stretching vibration, and the latter one appeared due to the C–C bond of PVDF [37,38]. In addition, two weak bands also appeared at 510 and 487 cm^{-1} which
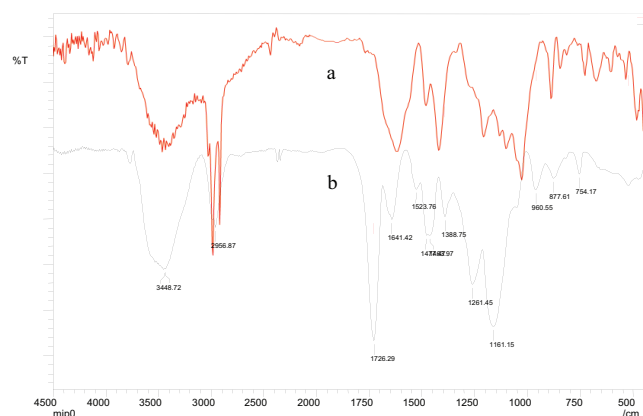

Fig. 2. FTIR spectrum of (a) PVDF nanofiber and (b) NFMIPs.

were assigned to the CF_2 bending vibration. After treatment of PVDF nanofiber, remarkable changes occurred in PVDF nanofiber. It can be seen from Fig. 2(b) that the NFMIPs exhibited an asymmetric and symmetric C–H stretching bands of –CH at a wavelength of 2,956.87 and 2,839 cm^{-1}, respectively. The stronger bands at about 1,728.22 cm^{-1} indicated the stretching vibrations band of C=O, while the peaks at 1,475.54 and 1,161.15 cm^{-1} were assigned to the stretching vibration bands of $–CH_3$ and $–O–CH_3$, respectively. However, other characteristic bands of NFMIPs were significantly overlapped with the absorption bands of PVDF nanofiber.

The crystalline structure of PVDF nanofiber and NFMIPs was characterized by XRD as shown in Fig. 3. A strong diffraction peak for PVDF nanofiber samples was observed at $2\theta = 20.7°$ corresponding to β (110) and β (200) planes. Weaker diffraction peaks at 36.7° and 41.1° assigned to β (201) and β (111) planes were also present [37,39]. These results indicate that electrospun nanofiber contains mainly β-phase crystal structure of PVDF, which may be formed during the preparation of electrospinning solution with DMF under 60°C. Previous study reported that PVDF could be crystallized with β-phase from DMF solution at 60°C [37,40]. In the XRD pattern of as prepared, NFMIPs exhibited clear diffraction peaks at 20°, 27° and 40° of 2θ and apparent diffraction peaks at 18.3°, 26.4°, 36.4° and 38.6° of 2θ (Fig. 3(b)). However, both electrospun PVDF nanofiber and NFMIPs only exhibited two clear diffraction peaks at 20.0° and 22.4° of 2θ. The clear diffractions could represent the perfection of α and β crystalline forms appearing in both materials. These revealed that the crystal structure of PVDF in NFMIPs does not change.

The surface morphologies of PVDF nanofiber membrane and NFMIPs material were observed by SEM and transmission electron microscopy (TEM). It can be seen from Figs. 4(a) and (c) that the PVDF nanofiber membrane has an ultrafine fiber with the diameter distributed mainly in range of 275–350 nm. For NFMIPs, the fiber showed uneven surface and the diameter was found to increase in the range of 295–393 nm. The existence of MIPs on the surface of the NFMIPs material was proven by TEM analysis in which
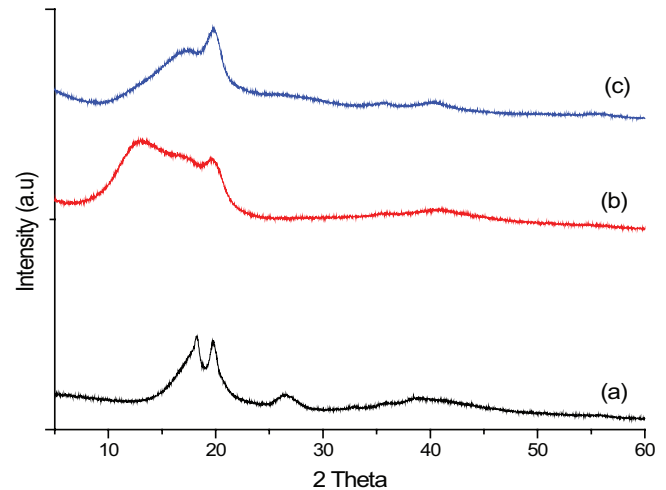

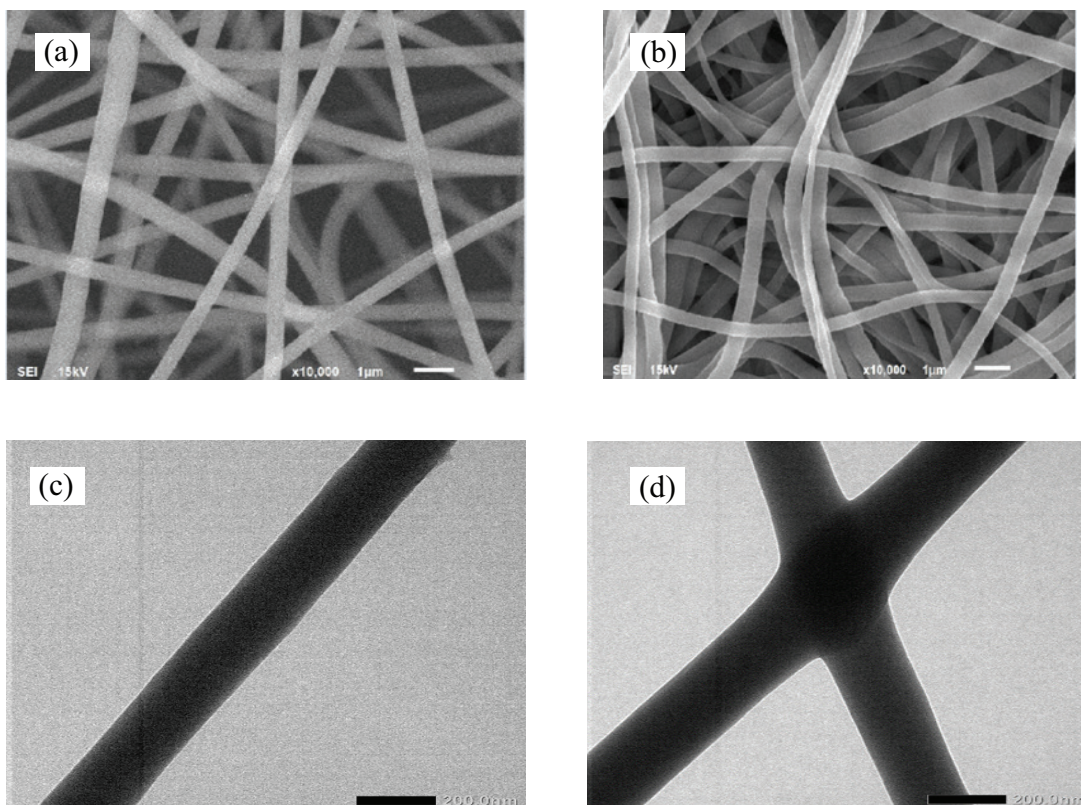Fig. 3. XRD pattern of (a) PVDF powder, (b) PVDF nanofiber and (c) NFMIPs.

Fig. 4. SEM images of (a) PVDF nanofiber and (b) NFMIPs; and TEM images of (c) PVDF nanofiber and (d) NFMIPs.

MIPs layer were successfully formed on the PVDF nanofibers surfaces as a layer with a thickness of about 43 nm (Fig. 4(d)).

The characteristics of the PVDF nanofiber membrane/ NFMIPs material are shown in Table 2. It can be seen that the mean pore size and maximal pore size of the NFMIPs are reduced significantly than original PVDF nanofiber membranes. It may be as a result of the relatively dense layer on the NFMIPs surface reducing a lot of membrane pore size. The BET analysis revealed that the surface area of the nanofiber decreased from 630.4 m²/g for PVDF nanofiber to 426.2 m²/g for NFMIPs (Table 2).

3.2. Adsorption studies

3.2.1. Effect of contact time

The effect of contact time on the adsorption of HA from peat water onto the PVDF nanofiber as well as NFMIPs in pH of solution with 25°C is shown in Fig. 5. As shown in the figure, the process of adsorption onto both nanofiber reached the equilibrium state after approximately 90 min of contact time. During the first 60 min, more than 80% of total adsorption of HA from peat water occurred which indicates that there were plenty of available adsorption sites. By continuing the process of adsorption, the adsorption sites were occupied gradually and the percentage removal was elevated slowly. Therefore, 90 min was selected as equilibrium time for further experiments.

3.2.2. Effect of adsorbent dosage

The effect of NFMIPs dosage on the HA adsorption from peat water is shown in Fig. 6. As can be seen, the percentage adsorption of HA raised with increasing NFMIPs dosage

up to a certain limit, then it reached a constant value. The increasing of the HA adsorption with the adsorbent dosage can be attributed to the increase of adsorbent surface area and the availability of more adsorption sites. It can be seen from Fig. 6 that the optimum percentage adsorption of HA occurred at adsorbent dosage of 0.05 g.

3.2.3. Effect of pH

The pH value of the peat water is an important factor for determination of the HA removal. The effect of the initial solution pH on the percentage adsorption of HA from peat water by NFMIPs is shown in Fig. 7. It is observed from Fig. 7 that the percentage adsorption decreases with increase in the pH of peat water from 2 to 10. The maximum adsorption of HA from peat water occurred at pH = 4.00. At this pH, a strong electrostatic interaction occurs between the positively charged adsorbent and the anionic HA molecules. The number of positively charged site of adsorbent decreased at high pH value and caused increasing repulsive forces between surface functional groups of adsorbent and HA compound. This phenomenon led to decreasing of percentage adsorption of HA [41–43].

Table 2
Characteristics of NFMIPs and PVDF nanofiber

Parameters	NFMIPs	PVDF nanofiber
BET surface area (m²/g)	426.2	630.4
Diameter range (nm)	295–393	275–350
Contact angle (°)	102.3	137.8

Fig. 6. Effect of adsorbent dosage on HA adsorption from peat water (contact time 90 min, volume 50 mL, pH 4.00, shaking speed 100 rpm and temperature 25°C).
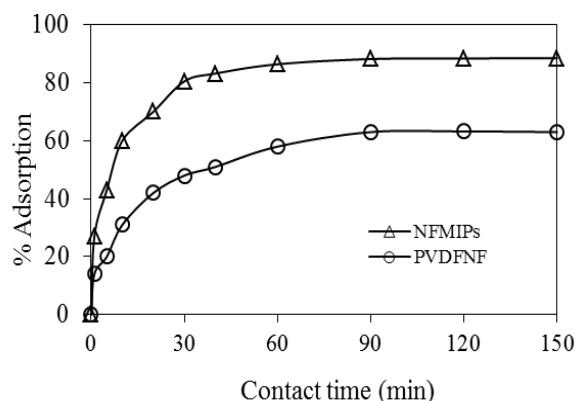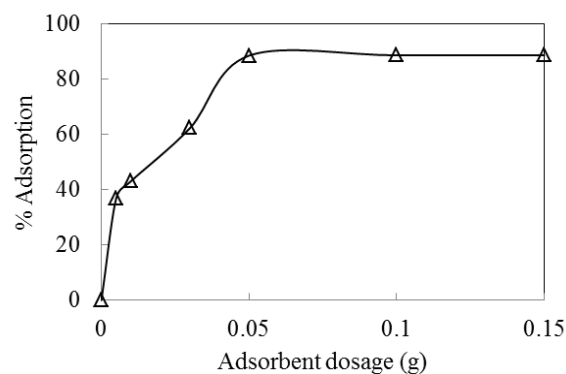

Fig. 5. Effect of contact time on HA adsorption from peat water (volume 50 mL, dosage 0.05 g, pH 4.00, shaking speed 100 rpm and temperature 25°C).
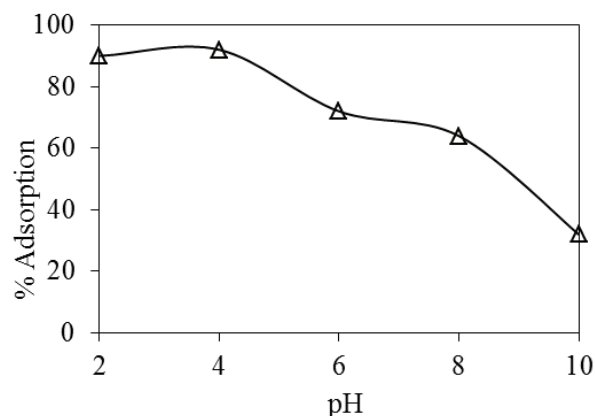

Fig. 7. Effect of pHs on HA removal from peat water (contact time 90 min, volume 50 mL, dosage 0.05 g, shaking speed 100 rpm and temperature 25°C).

3.2.4. Effect of temperature

Observation of temperature effect was performed to investigate the adsorption capacities of the adsorbents. According to the results, the adsorption amount of HA onto NFMIPs at equilibrium was also affected by temperature (figure not shown here). The adsorption amount increased as the temperature increased, indicating that favorable adsorption occurs at higher temperatures. The phenomenon may be due to the increase of diffusion rate and the mobility of HA molecules across the surface of the adsorbent. In other words, by raising the temperature, the adsorption capacity of NFMIPs can be increased [44,45]. This indicated that the adsorption of HA onto NFMIPs was controlled by an endothermic process.

3.2.5. Isotherm adsorption

Adsorption isotherms describe how adsorbates interact with adsorbents. Therefore, the correlation of equilibrium data by either theoretical or empirical equations is essential to the practical design and operation of adsorption systems [46]. In this case, the Langmuir, Freundlich and Sips equations were used to investigate the adsorption isotherms. Langmuir's model of adsorption depends on the assumption that intermolecular forces decrease rapidly with distance and consequently predicts the existence of monolayer coverage of the adsorbate at the outer surface of the adsorbent. The isotherm equation further assumes that adsorption takes place at specific homogeneous sites within the adsorbent. The non-linear Langmuir equation is represented as follows:

$$q_e = \frac{q_m b C_e}{1 + b C_e} \tag{3}$$

where C_e represents the equilibrium concentration (mg/L), q_e represents the amount adsorbed per amount of absorbent at the equilibrium (mg/g), q_m and b are the maximum adsorption capacity (mg/g) and Langmuir constant (L/mg), respectively.

The Freundlich adsorption equation was used to describe experimental adsorption data based on empirical equations which are used to describe multilayer adsorption involving interaction between adsorbed molecules. The Freundlich equation can be written as:

$$q_e = K_f C_e^{1/n} \tag{4}$$

where C_e represents the equilibrium concentration (mg/L), q_e represents the amount of adsorbed molecule per unit weight of absorbent (mg/g) and K_f and n are Freundlich constants. K_f value corresponds to adsorption capacity of the adsorbent, while $1/n$, varying between 0 and 1, corresponds to adsorption intensity or surface heterogeneity. Adsorption with n greater than one indicates that the process is categorized as a favorable adsorption process [47].

Sips isotherm is a combination of the Langmuir and Freundlich models and employed to analyze the equilibrium data obtained during batch adsorption studies. The equation is expressed in Eq. (5):

$$q_e = \frac{q_m K_{eq} C_e^n}{1 + K_{eq} C_e^n} \tag{5}$$

where K_{eq} (L/mg) is the equilibrium constant of Sips equation while q_m (mg/g) represents the maximum adsorption capacity and C_e is the equilibrium concentration (L/mg). Sips isotherm can be used to describe the heterogeneous system. The equation is characterized by the heterogeneity factor, n. When $n = 1$, Sips isotherm equation reduces to the Langmuir equation and it implies a homogeneous adsorption processes [48,49].

The isotherms of HA on the prepared NFMIPs predicted from all the three models were plotted in Fig. 8. All the correlation coefficient, R^2 values and the constants obtained for the models are summarized in Table 3. The Langmuir model yielded the best fit with the highest R^2 value of 0.997, thus the Langmuir isotherm was the most suitable equation to describe the adsorption equilibrium of HA on the NFMIPs. As can be seen from Fig. 8, the q_e values predicted from the Langmuir model agreed well with the experimental values. The suitability of the Langmuir isotherm to fit the data was confirmed by the $1/n$ value from Freundlich model, which was below 1, and also indicating a normal Langmuir isotherm [50]. Moreover, the adsorption of each adsorbate molecule onto the surface had equal adsorption activation energy and the maximum adsorption capacity (q_m) was 153.3 mg/g.
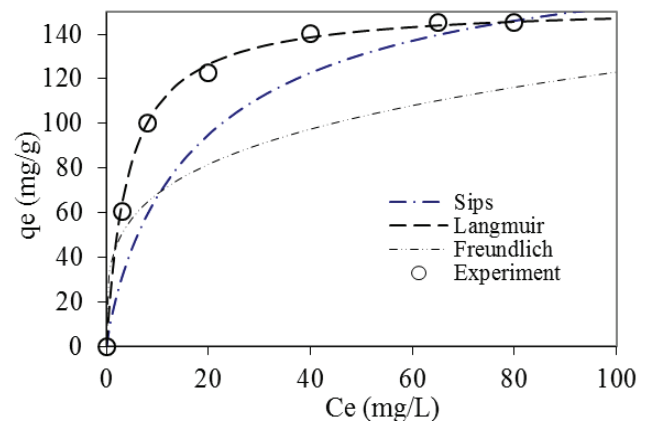

Fig. 8. Isotherm curve for HA removal from peat water (contact time 90 min, volume 50 mL, dosage 0.05 g, shaking speed 100 rpm and temperature 25°C).

Table 3
Langmuir, Freundlich and Sips parameters for HA adsorption onto NFMIPs

Langmuir model			Freundlich model			Sips model			
b (L/mg)	q_m (mg/g)	R^2	n	K_f (mg/g)	R^2	q_m (mg/g)	K_{eq} (mL/g)	n	R^2
0.236	153.3	0.997	3.94	38.2	0.967	150.2	0.095	0.884	0.988

3.2.6. Adsorption kinetics

Generally, three steps are involved during the process of adsorption by porous adsorbent particles: external mass transfer, interparticle transport and chemisorption [51]. Several kinetic models have been proposed to clarify the mechanism of a solute sorption from aqueous solution onto an adsorbent: pseudo-first-order kinetic model of Lagergren, pseudo-second-order kinetic model of Ho and intraparticle diffusion model of Weber and Morris. In this work, adsorption kinetics of HA onto NFMIPs was studied in terms of pseudo-first-order and pseudo-second-order models. The pseudo-first-order kinetic model is shown in Eq. (6):

$$\log(q_e - q_t) = \log q_e - (k_1/2.303)\, t \tag{6}$$

where q_e is the adsorption capacity (mg/g) at equilibrium, q_t is the adsorption capacity (mg/g) at time, t (min) and k_1 (min^{-1}) is the Lagergren rate constant of adsorption. The values of k_1 and q_e were determined from the intercept and the slope of the linear plots of $\log(q_e - q_t)$ vs. t (Fig. 9(a)). The rate constant k_1, q_e and the correlation coefficient for this kinetic model are presented in Table 4.

The pseudo-second-order kinetic model is also analyzed to fit the data and is given by:

$$t/q_t = 1/k_2 q_e^2 + t/q_e \tag{7}$$

where k_2 (g/mg min) is pseudo-second-order rate constant of adsorption. For this model, k_2 and q_e (Table 4) were determined from the intercept and the slope of the linear plot of (t/q_t) vs. t (Fig. 9(b)).

From Fig. 9(b), it was observed that the pseudo-second-order kinetic model adequately fit the experimental values. These results suggest that HA adsorption onto NFMIPs follows the pseudo-second-order kinetic model. This means that chemisorption is the rate-determining step and the overall rate of HA adsorption process seems to be controlled by the chemical process through exchanging of electrons between adsorbent and adsorbate [45,52]. Also from Table 4, it is indicated that the calculated equilibrium adsorption capacity (q_e) values of the pseudo-second-order model agree well with the experimental data.

Adsorption kinetics was controlled by adsorption mechanism and rate-limiting step of the process. In general, the adsorption of adsorbate onto the adsorbents can occur through three consecutive steps: (1) mass transfer of adsorbate from boundary film to the surface of resin (film diffusion); (2) mass transport of adsorbate molecules within the pores of resin (intraparticle diffusion) and (3) adsorption of the adsorbate molecules on the interior surface of resin. The third step is a fast and non-limiting step in the adsorption process. So the adsorption rate can be limited by the first (film diffusion) and/or the second steps (intraparticle diffusion) [23,53,54].

To investigate the mechanism of adsorption of HA onto NFMIPs, the intraparticle diffusion and Boyd kinetic models is used. The intraparticle diffusion model can be defined as:

$$q_t = k_d t^{1/2} + C \tag{8}$$

where k_d and C are an intraparticle diffusion rate constant (mg g^{-1} min$^{-1/2}$) and a constant, respectively. The value of k_d and C can be determined from the slope and intercepts of the straight line. If the plot of q_t vs. $t^{1/2}$ gives a straight line and
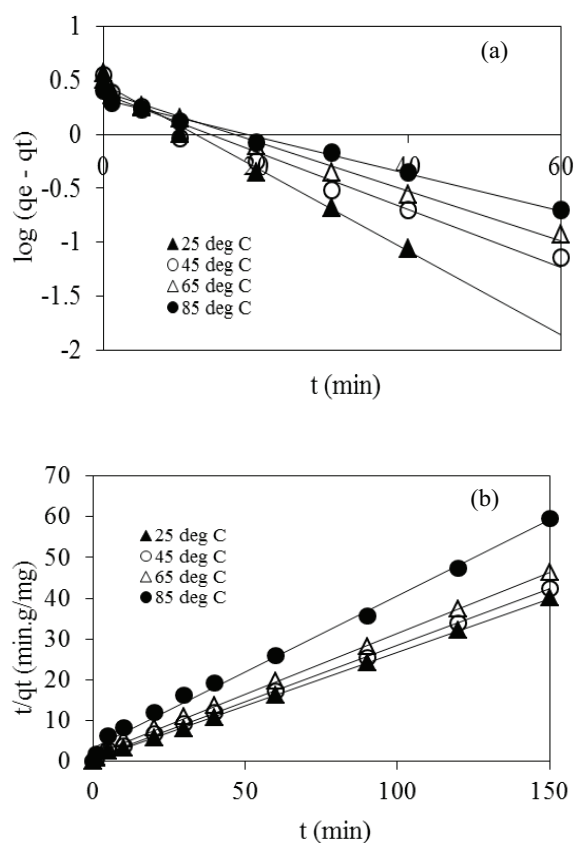

Fig. 9. (a) Pseudo-first-order and (b) pseudo-second-order model plots for HA removal from peat water at different temperature (volume 50 mL, dosage 0.05 g and shaking speed 100 rpm).

Table 4
Pseudo-first-order and pseudo-second-order kinetics parameters for HA adsorption onto NFMIPs

Temperature (°C)	Pseudo-first-order			Pseudo-second-order			
	k_1 (min^{-1})	$q_{e,\text{cal}}$ (mg/g)	R^2	k_2 (g/mg min)	$q_{e,\text{cal}}$ (mg/g)	R^2	$q_{e,\text{exp}}$ (mg/g)
25	0.040	2.123	0.991	0.043	2.677	0.999	2.520
45	0.053	2.490	0.969	0.056	3.347	0.999	3.200
65	0.062	2.378	0.987	0.087	3.622	0.998	3.528
85	0.089	2.917	0.989	0.156	3.794	0.995	3.728

passed through the origin, the adsorption process of HA is controlled by intraparticle diffusion only. From the plot of q_t against $t^{1/2}$, it can be seen that these plots generally have a dual nature, implying that more than one process affected the sorption (Fig. 10). From these figure, it is clear that at all temperatures, the adsorption processes of the HA follows two phases, suggesting that the intraparticle diffusion (or pore diffusion) is not the rate-limiting step for the entire reaction. The initial portion of the plot indicated an external mass transfer (or film diffusion) whereas the second linear portion is due to intraparticle or pore diffusion. Extrapolating the linear portion of the plot to the ordinate produces the intercept (C) which is proportional to the extent of boundary layer thickness [14,21–23,48]. The values of k_{d1} and k_{d2} as obtained from the slopes of the two straight lines are listed in Table 5.

The values of k_{d1} and k_{d2} for the adsorption of HA slightly increased with increasing temperature from 25°C to 85°C. This indicated that increasing temperature slightly increases the migration of HA into the inner structure of the NFMIPs. From Table 5, we also can see that the value of C increased with increasing temperature. This suggests that the effect of boundary layer diffusion for the adsorption of HA on the NFMIPs probably become more important at higher temperature because of the greater random motion associated with the increased thermal energy [22,23].

The other thermodynamic parameter is activation energy (E_a). The Arrhenius equation was applied to evaluate the E_a of the adsorption process:

$$\ln k = \ln A - \frac{E_a}{RT} \tag{9}$$

where k is rate constant of pseudo-second-order kinetic model (g/mg min), E_a is the activation energy (kJ/mol), A is the Arrhenius factor, R is the gas constant (8.314 J/mol K) and T is the solution absolute temperature (K). The linear plot of $\ln k$ vs. $1/T$ gives a straight line with slope $-E_a/R$. The activation energy obtained in this study was 19.43 kJ/mol. The positive value of E_a suggests that an increase in temperature favors the adsorption of HA onto NFMIPs, and that the adsorption process is endothermic in nature [22,23].

4. Conclusion

A NFMIPs was successfully prepared by the electrospinning technique for the HA removal from peat water. The characterization of synthesized PVDF nanofiber and NFMIPs was performed using XRD, FTIR, SEM, TEM, BET and contact angle. Characterization results indicated that MIPs were successfully coated onto the surface of the PVDF nanofiber and did not cause any changes in its structure. The results of the present study also clearly suggest that NFMIPs can be successfully utilized for the removal of HA from peat water. The sorption capacity is strongly dependent on the contact time, adsorbent dosage, pH and temperatures. Adsorption isotherms were better fitted by Langmuir isotherm in which the adsorption capacity was found to be 153.3 mg/g. The kinetic process of HA adsorption onto NFMIPs was found to fit the pseudo-second-order rate equation with a rate constant in the range of 0.032–0.104 g/mg min.
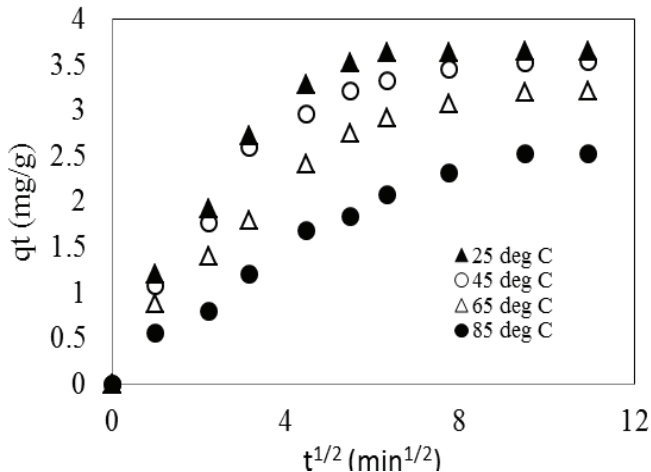
Fig. 10. Intraparticle diffusion model plot for HA removal from peat water at different temperature (volume 50 mL, dosage 0.05 g and shaking speed 100 rpm).

Table 5
Parameter of the intraparticle diffusion model for HA adsorption onto NFMIPs

Temperature (°C)	k_{d1} (mg g^{-1} min$^{-1/2}$)	C_1	k_{d2} (mg g^{-1} min$^{-1/2}$)	C_2
25	0.334	0.103	0.043	2.042
45	0.483	0.223	0.033	2.845
65	0.580	0.356	0.018	3.333
85	0.634	0.379	0.043	3.608

References

[1] J. Wang, X. Han, H. Ma, Y. Ji, L. Bi, Adsorptive removal of humic acid from aqueous solution on polyaniline/attapulgite composite, Chem. Eng. J., 173 (2013) 171–177.
[2] D. Sonea, R. Pode, F. Manea, C. Ratiu, C. Lazau, I. Grozescu, G. Burtica, The comparative assessment of photolysis, sorption and photocatalysis processes to humic acids removal from water, Chem. Bull. "POLITEHNICA" Univ. (Timisoara), 55 (2010) 148–151.
[3] D. Ghernaout, B. Ghernaout, A. Saibaa, A. Boucherita, A. Kellil, Removal of humic acids by continuous electromagnetic treatment followed by electrocoagulation in batch using aluminium electrodes, Desalination, 239 (2009) 295–308.
[4] F.X. Simon, E. Rudé, J. Llorens, S. Baig, Study on the removal of biodegradable NOM from seawater using biofiltration, Desalination, 316 (2013) 8–16.
[5] J.C. Rojas, J. Pérez, G. Garralón, F. Plaza, B. Moreno, M.A. Gómez, Humic acids removal by aerated spiral-wound ultrafiltration membrane combined with coagulation–hydraulic flocculation, Desalination, 266 (2011) 128–133.
[6] I. Gutman, D. Hasson, R. Semiat, Humic substances fouling in ultrafiltration processes, Desalination, 261 (2010) 218–231.

[7] J.W. Kim, W.J. Cho, C.S. Ha, Morphology, crystalline structure, and properties of poly(vinylidene fluoride)/silica hybrid composites, J. Polym. Sci., Part B: Polym. Phys., 40 (2002) 19–30.

[8] P. Malik, Use of activated carbons prepared from sawdust and rice-husk for adsorption of acid dyes: a case study of Acid Yellow 36, Dyes Pigm., 56 (2003) 239–249.

[9] M. Toor, B. Jin, Adsorption characteristics, isotherm, kinetics, and diffusion of modified natural bentonite for removing diazo dye, Chem. Eng. J., 187 (2012) 79–88.

[10] M.A.F. García, J.R. Utrilla, I.B. Toledo, C.M. Castilla, Adsorption of humic substances on activated carbon from aqueous solutions and their effect on the removal of Cr(III) ions, Langmuir, 14 (1998) 1880–1886.

[11] A.A.M. Daifullah, B.S. Girgis, H.M.H. Gad, A study of the factors affecting the removal of humic acid by activated carbon prepared from biomass material, Colloids Surf., A, 235 (2004) 1–10.

[12] S. Wang, Z.H. Zhu, Humic acid adsorption on fly ash and its derived unburned carbon, J. Colloid Interface Sci., 315 (2007) 41–46.

[13] A. Kamari, W.S.W. Ngah, L. Wong, Shorea dasyphylla sawdust for humic acid sorption, Eur. J. Wood Wood Prod., 67 (2009) 417–426.

[14] M.A. Zulfikar, E. Novita, R. Hertadi, S.D. Djajanti, Removal of humic acid from peat water using untreated powdered eggshell as a low cost adsorbent, Int. J. Environ. Sci. Technol., 10 (2013) 1357–1366.

[15] G.K. Moussavi, Removal of petroleum hydrocarbons from contaminated groundwater using an electrocoagulation process: batch and continuous experiments, Desalination, 278 (2011) 288–294.

[16] C. Leodopoulos, D. Doulia, K. Gimouhopoulos, T. Triantis, Single and simultaneous adsorption of methyl orange and humic acid onto bentonite, Appl. Clay Sci., 70 (2012) 84–90.

[17] L. Zhang, L. Luo, S. Zhang, Integrated investigations on the adsorption mechanisms of fulvic and humic acids on three clay minerals, Colloids Surf., A, 406 (2012) 84–90.

[18] W.S.W. Ngah, A. Musa, Adsorption of humic acid onto chitin and chitosan, J. Appl. Polym. Sci., 69 (1998) 2305–2310.

[19] W.S.W. Ngah, S. Fatinathan, N.A. Yosop, Isotherm and kinetic studies on the adsorption of humic acid onto chitosan-H_2SO_4 beads, Desalination, 272 (2011) 293–300.

[20] L. Liang, L. Luo, S. Zhang, Adsorption and desorption of humic and fulvic acids on SiO_2 particles at nano- and micro-scales, Colloids Surf., A, 384 (2011) 126–130.

[21] Q. Tao, Z. Xu, J. Wang, F. Liu, H. Wan, S. Zheng, Adsorption of humic acid to aminopropyl functionalized SBA-15, Microporous Mesoporous Mater., 131 (2010) 177–185.

[22] J. Lin, Y. Zhan, Adsorption of humic acid from aqueous solution onto unmodified and surfactant-modified chitosan/zeolite composites, Chem. Eng. J., 200–202 (2012) 202–213.

[23] M.A. Zulfikar, D. Wahyuningrum, R. Mukti, H. Setiyanto, Molecularly imprinted polymers (MIPs): a functional material for removal of humic acid from peat water, Desal. Wat. Treat., 57 (2016) 15164–15175.

[24] Z. Ma, S. Ramakrishna, Electrospun regenerated cellulose nanofiber affinity membrane functionalized with protein A/G for IgG purification, J. Membr. Sci., 319 (2008) 23–28.

[25] H. Zhang, H. Nie, D. Yu, C. Wu, Y. Zhang, C. White, Surface modification of electrospun polyacrylonitrile nanofiber towards developing an affinity membrane for bromelain adsorption, Desalination, 256 (2010) 141–147.

[26] M. Aliabadi, M. Irani, J. Ismaeili, H. Piri, M. Parnian, Electrospun nanofiber membrane of PEO/Chitosan for the adsorption of nickel, cadmium, lead and copper ions from aqueous solution, Chem. Eng. J., 220 (2013) 237–243.

[27] M. Aliabadi, M. Irani, J. Ismaeili, S. Najafzadeh, Design and evaluation of chitosan/hydroxyapatite composite nanofiber membrane for the removal of heavy metal ions from aqueous solution, J. Taiwan Inst. Chem. Eng., 45 (2014) 518.

[28] D. Sharma, F. Li, Y. Wu, Electrospinning of Nafion and polyvinyl alcohol into nanofiber membranes: a facile approach to fabricate functional adsorbent for heavy metals, Colloids Surf., A, 457 (2014) 236–243.

[29] C. Peng, J. Zhang, Z. Xiong, B. Zhao, P. Liu, Fabrication of porous hollow-Al_2O_3 nanofibers by facile electrospinning and its application for water remediation, Microporous Mesoporous Mater., 215 (2015) 133–142.

[30] Q. Xin, J. Fua, Z. Chen, S. Liu, Y. Yan, J. Zhang, Polypyrrole nanofibers as a high-efficient adsorbent for the removal of methyl orange from aqueous solution, J. Environ. Chem. Eng., 3 (2015) 1637–1647.

[31] R. Xu, M. Jia, Y. Zhang, F. Li, Sorption of malachite green on vinyl-modified mesoporous poly(acrylic acid)/SiO_2 composite nanofiber membranes, Microporous Mesoporous Mater., 149 (2012) 111–118.

[32] R. Rajkumar, A. Warsinke, H. Mohwald, F. Scheller, M. Katterle, Analysis of recognition of fructose by imprinted polymers, Talanta, 75 (2008) 1119–1123.

[33] W. Yang, L. Liu, W. Zhou, W. Xu, Z. Zhou, W. Huang, Preparation and evaluation of hollow molecular imprinted polymer for adsorption of dibenzothiophene, Appl. Surf. Sci., 258 (2012) 6583–6589.

[34] X. He, F. Gao, G. Tu, D. Hasko, S. Huttner, U. Steiner, Formation of nano patterned polymer blends in photovoltaic devices, Nano Lett., 10 (2010) 1302–1307.

[35] B. Prasad, R. Madhuri, M. Tiwari, P. Sharma, Imprinting molecular recognition sites on multiwalled carbon nanotubes surface for electrochemical detection of insulin in real samples, Electrochim. Acta, 55 (2010) 9146–9156.

[36] C. Gao, S. Deng, J. Wan, B. Lu, R. Liu, E. Huq, 22 nm silicon nanowire gas sensor fabricated by trilayer nanoimprint and wet etching, Microelectron. Eng., 87 (2010) 927–930.

[37] Y. Kim, C. Ahn, M. Lee, M. Choi, Characteristics of electrospun PVDF/SiO_2 composite nanofiber membranes as polymer electrolyte, Mater. Chem. Phys., 127 (2011) 137–142.

[38] A. Rahimpour, S. Madaeni, S. Zereshki, Y. Mansourpanah, Preparation and characterization of modified nano-porous PVDF membrane with high antifouling property using UV photo-grafting, Appl. Surf. Sci., 255 (2009) 7455–7461.

[39] P. Sukitpaneenit, T. Chung, Molecular elucidation of morphology and mechanical properties of PVDF hollow fiber membranes from aspects of phase inversion, crystallization and rheology, J. Membr. Sci., 340 (2009) 192–205.

[40] R. Gregorio, E. Uemo, Effect of crystalline phase, orientation and temperature on the dielectric properties of poly (vinylidene fluoride) (PVDF), J. Mater. Sci., 34 (1999) 4489–4500.

[41] J.M. Bandara, Molecular mechanism of surface recognition. Azo dyes degradation on Fe, Ti, and Al oxides through metal sulfonate complexes, Langmuir, 15 (1999) 7670–7679.

[42] M. Do, N. Phan, T. Nguyen, T. Pham, V. Nguyen, T. Vu, Activated carbon/Fe_3O_4 nanoparticle composite: fabrication, methyl orange removal and regeneration by hydrogen peroxide, Chemosphere, 85 (2011) 1269–1276.

[43] A.G. Rodríguez, Adsorption of anionic and cationic dyes on activated carbon from aqueous solutions: equilibrium and kinetics, J. Hazard. Mater., 172 (2009) 1311–1320.

[44] L. Ai, C. Zhang, F. Liao, Y. Wang, M. Li, L. Meng, Removal of methylene blue from aqueous solution with magnetite loaded multi-wall carbon nanotube: kinetic, isotherm and mechanism analysis, J. Hazard. Mater., 198 (2011) 282–290.

[45] A. Mohammadi, H. Daemi, M. Barikani, Fast removal of malachite green dye using novel superparamagnetic sodium alginate-coated Fe_3O_4 nanoparticles, Int. J. Biol. Macromol., 69 (2014) 447–455.

[46] C.H. Xiong, C.P. Yao, Study on the adsorption of cadmium(II) from aqueous solution by D152 resin, J. Hazard. Mater., 166 (2009) 815–820.

[47] C.L. Ng, Freundlich adsorption isotherms of agricultural by-product-based powdered activated carbons in a geosmin-water system, Bioresour. Technol., 85 (2002) 131–135.

[48] M.A. Zulfikar, D. Wahyuningrum, S. Lestari, Adsorption of lignosulfonate compound from aqueous solution onto chitosan-silica beads, Sep. Sci. Technol., 48 (2013) 1391–1401.

[49] M.M. Benedetti, Metal ion binding to humic substances: application of the non-ideal competitive adsorption model, Environ. Sci.Technol., 29 (1995) 446–457.

[50] B.H. Hameed, I.A.W. Tan, A.L. Ahmad, Adsorption isotherm, kinetic modeling and mechanism of 2,4,6-trichlorophenol on coconut husk-based activated carbon, Chem. Eng. J., 144 (2008) 235–244.

[51] W. Wang, B. Zheng, Z. Deng, Z. Feng, L. Fu, Kinetics and equilibriums for adsorption of poly(vinyl alcohol) from aqueous solution onto natural bentonite, Chem. Eng. J., 214 (2013) 343–354.

[52] Y. Nuhoglu, E. Malkoc, Thermodynamic and kinetic studies for environmentaly friendly Ni(II) biosorption using waste pomace of olive oil factory, Bioresour. Technol., 100 (2009) 2375–2380.

[53] Z.P. Gao, Z.F. Yu, T.L. Yue, S.Y. Quek, Adsorption isotherm, thermodynamics and kinetics studies of polyphenols separation from kiwifruit juice using adsorbent resin, J. Food Eng., 116 (2013) 195–201.

[54] Y.S. Ho, G. McKay, Competitive sorption of copper and nickel ions from aqueous solution using peat, Adsorption, 5 (1999) 409–417.